

1 **Numerical Modeling of the Morphodynamic Response of a Low-lying Barrier Island Beach and**
2 **Foredune System Inundated during Hurricane Ike using XBeach and CSHORE**

3

4

CRAIG HARTER¹ and JENS FIGLUS²

5

6 1. *Zachry Department of Civil Engineering, Ocean Engineering Division, Texas A&M University, 3136 TAMU, College*

7

Station, TX, USA. craig.harter@tamu.edu.

8

2. *Department of Ocean Engineering, Texas A&M University – Galveston Campus, 200 Seawolf Pkwy., Galveston, TX, USA.*

9

figlusj@tamug.edu.

10 **Abstract**

11 Follet's Island (FI) is a sediment-starved barrier island located on the Upper Texas Coast; a
12 stretch of coastline along the Gulf of Mexico that experiences on average four hurricanes and
13 four tropical storms per decade. During Hurricane Ike, water levels and wave heights at FI
14 exceeded the 100-year and 40-year return values, respectively, leading to significant overtopping
15 and morphology changes of this low-lying barrier island. The physical processes governing the
16 real-time morphodynamic response of the beach and dune system during 96 hours of hurricane
17 impact were modeled using XBeach (2D) and CSHORE (1D). Hydrodynamic boundary
18 conditions were obtained from ADCIRC/SWAN model runs validated with measured buoy and
19 wave gauge data while LiDAR surveys provided pre- and post-storm measured topography.

20 XBeach displayed a decent model skill of 0.34 and provided numerical outputs of the entire 2D
21 domain such as topography, suspended sediment load and bed load which was very useful in
22 visualizing erosion and deposition patterns. CSHORE also displayed a decent model skill of 0.33
23 and was able to accurately predict the post-storm beach slope and shoreline, but was less
24 effective at simulating the foredune morphology. Modeling results show that the complete

25 morphodynamic response of FI to Hurricane Ike was governed by a sequence of impact regimes,
26 including swash, collision, overwash, inundation, and storm surge ebb.

27 **1. Background and Motivation**

28 In many places along the U.S. East and Gulf Coast, barrier islands are the first line of defense
29 against extreme weather events threatening our coastlines. The morphological evolution of
30 barrier islands depends on both long-term and short-term processes and is inherently linked to
31 local sediment availability (Zhang, 2002; Leatherman et al., 1983). Many researchers have
32 discussed long-term and short-term morphology changes of barrier islands with different focus
33 areas (e.g. Morton and Sallenger, 2003; Rosati and Stone, 2009, Wang et al., 2006, Houser et al.
34 2008), a detailed review of which is beyond the scope of this paper. Unfortunately, only limited
35 data are available to quantify or predict the morphological evolution of barrier islands. The goal
36 of this study is to better understand the dynamics of morphological changes in barrier island
37 systems caused by extreme events since their compounding effects play a critical role in the
38 long-term evolutionary trends of our coastlines and a better understanding of the governing
39 processes will lead to improved coastal management strategies. As a case study, Follet's Island
40 (FI), a sediment-starved barrier island along the Upper Texas Coast (UTC) is examined (Fig. 1).

41 The forcing conditions driving the morphodynamics of barrier islands during storms are
42 characterized by four impact regimes as outlined by Sallenger (2000): swash, collision, overwash
43 and inundation. During the swash regime, swash motions reach only as high as the dune toe, and
44 sediment is pulled from the beach offshore. The collision regime is characterized by waves
45 directly impacting and eroding the dune face. During the overwash regime, wave runup levels
46 exceed the dune crest, allowing washover sediments to be deposited on the back side of the dune.

47 Finally, during the inundation regime, the storm surge level exceeds the dune crest causing high
48 velocity overwash flows and wave penetration to the back-bay.

49 Follet's island experienced all of these regimes during the passage of Hurricane Ike in
50 2008, including a prolonged collision regime due to a forerunner surge that preceded the storm
51 surge (Kennedy et al., 2011). Additionally, Follet's Island experienced significant morphological
52 changes due to the ebbing storm surge after the hurricane made landfall. This additional
53 morphodynamic forcing condition caused by gravity-driven flow from the bay to the
54 ocean has been investigated by several researchers (e.g. Hayes, 1967; Thieler and
55 Bush, 1991; Lennon, 1991, Tedesco et al., 1995; Goff et al., 2010; and Sherwood et al.,
56 2014). The significant gradient between bay and ocean water levels after passing of a
57 storm can scour previously deposited material and potentially affect the sediment
58 budget of the beach-barrier-bay system due to this offshore sediment transport
59 mechanism.

60 Storm surge at FI reached a peak storm elevation of 2.6 m NAVD88, which exceeded
61 the 100-year high water level. This peak was preceded by a forerunner surge of about 1
62 m beginning approximately 18 hours before landfall, after which the water level steadily
63 rose to 2.2 m NAVD88 over the next 12 hours. This flooded Christmas Bay and the
64 back barrier region well before Ike made landfall. Waves offshore of FI exceeded 4.5 m
65 significant wave height at 16 second peak period; roughly the 40-year wave conditions.
66 After landfall, the water level quickly dropped to 2 m NAVD88 over the course of 12
67 hours. The amount of inland flooding from the forerunner resulted in a strong ebb flow
68 that scoured large channels in FI as the water dragged sediment back out to the gulf.

69 The UTC is characterized by a series of long, narrow barrier islands and barrier peninsulas
70 comprised of fine sand, and a microtidal, wave-dominated hydrodynamic environment (Morton
71 et al., 1994; Mason, 1981). FI is one of the most vulnerable stretches of the UTC due to its lack
72 of a major sediment source and high background erosion rates (Paine et al., 2012). The island is
73 approximately 25 km long, less than 500 m wide and 2.06 m in elevation (NAVD88), and
74 contains a series of beach communities, including Treasure Island and Surfside. In addition, FI
75 protects important economic and ecological assets like Christmas Bay, the Brazoria National
76 Wildlife Refuge, the CR-257 Blue Water Highway, the Gulf Intracoastal Waterway (GIWW),
77 and parts of the port of Freeport including the Naval Petroleum Reserve and an LNG de-
78 liquification plant (Fig. 1).

79 In 1929, the Brazos River was rerouted 6.5 miles west of the Freeport jetties. The Brazos River
80 was formerly a major sediment source for FI, and its rerouting in conjunction with damming
81 upriver resulted in a sediment deficit on FI (Morton and Pieper, 1975; Mason, 1981). As a result,
82 FI experiences high rates of background erosion due to cross- and alongshore transport, with
83 shoreline retreat rates between -1.5 m/yr and -3.9 m/yr (Paine et al., 2012).

84 In this study we observe the impact of the hurricane on the subaerial morphology of FI
85 comparing results from the coastal response numerical models, XBeach (Roelvink, 2009) and
86 CSHORE (Johnson et al., 2012; Kobayashi, 2013). While both numerical models utilize process-
87 based techniques to compute short-term beach and dune morphology evolution, the two
88 approaches differ greatly from each other. The motivation to compare results from these two
89 inherently different model approaches to each other using a specific case study is manifold. Both
90 numerical models have received funding for development through the U.S. Army Corps of
91 Engineers MORPHOS project but to the authors' knowledge no direct comparison between them

92 using field data has been published. Both models have become widely-used free-ware tools in
93 academia, government agencies, and industry to assess storm impact on sandy coastline
94 morphology. This comparative case study intends to highlight capabilities and shortcomings of
95 both models using mostly default model parameters. Specifically, the trade-off between using a
96 2D model with greater spatial coverage and more resolved hydrodynamics but significantly
97 higher computational cost versus a cross-shore depth-averaged probability-based model with
98 only a fraction of the computational cost.

99 **2. Numerical Models**

100 ***2.1. XBeach Background***

101 XBeach is a powerful numerical modeling tool developed for simulating the coastal response of
102 sandy beach systems to time-varying storm conditions (Roelvink, 2009, Roelvink et al., 2010).
103 The model was built to simulate physical processes within different impact regimes of a storm as
104 defined by Sallenger: (1) swash regime, (2) collision regime, (3) overwash regime, (4)
105 inundation regime (Sallenger, 2000). For resolving swash dynamics, the model incorporates a
106 2DH description of wave groups from the time-varying wave action balance. This wave-group
107 forcing drives infragravity (IG) motions, including both longshore and cross-shore currents. In
108 the collision regime, an avalanching model is used to transport sediment from the dune face (dry)
109 to the swash zone (wet), incorporating the fact that saturated sand moves more readily than dry
110 sand. This is achieved by identifying a critical slope for both wet and dry conditions. For the
111 overwash regime, wave group forcing of low frequency motions is applied with a robust
112 momentum-conserving drying/flooding formulation and sediment transport formulation. Finally,
113 the inundation regime includes a semi-empirical model for breach evolution based on a

114 schematic uniform cross-section.

115 XBeach includes routines for short-wave envelope propagation (refraction and shoaling), non-
116 stationary shallow water equations, undertow, and non-cohesive sediment transport and bed
117 update, including avalanching, dune erosion, overwash, and breaching. The model includes a
118 time-dependent wave action balance solver, eliminating the need for a separate wave model and
119 allowing different wave groups to travel in different directions. The wave action balance is
120 defined as:

$$\frac{\partial A}{\partial t} + \frac{\partial c_x A}{\partial x} + \frac{\partial c_y A}{\partial y} + \frac{\partial c_\theta A}{\partial \theta} = -\frac{D_w}{\sigma} \quad (1)$$

121 where the wave action, A , is defined by:

$$A(x, y, t, \theta) = \frac{S_w(x, y, t, \theta)}{\sigma(x, y, t)} \quad (2)$$

122 and where S_w represents the wave energy density in each directional bin, θ represents the angle
123 of incidence with respect to the x -axis, σ represents the intrinsic wave frequency, D_w represents
124 the wave energy dissipation, and c_x , c_y , and c_θ represent the wave action propagation speeds in x -
125 , y -, and θ - space respectively.

126 The roller energy balance is coupled to the wave action balance based on the wave energy
127 dissipation, D_w , and is defined as:

$$\frac{\partial S_r}{\partial t} + \frac{\partial c_x S_r}{\partial x} + \frac{\partial c_y S_r}{\partial y} + \frac{\partial c_\theta S_r}{\partial \theta} = -D_r + D_w \quad (3)$$

128 where $S_r(x,y,t,\theta)$ represents the roller energy in each directional bin, and D_r represents the total
 129 roller energy. Radiation stresses from the roller energy balance and the wave action balance are
 130 added together to calculate the radiation stress tensor used in the shallow water equation solver.
 131 For low frequency and mean flows, the shallow water equations are built into a depth-averaged
 132 Generalized Lagrangian Mean (GLM) formulation. These equations are based on the Lagrangian
 133 velocity, which in this context is equivalent to the Eulerian velocity plus the Stokes drift. The
 134 equations are summarized as:

$$\frac{\partial u^L}{\partial t} + u^L \frac{\partial u^L}{\partial x} + v^L \frac{\partial u^L}{\partial y} - f v^L - v_h \left(\frac{\partial^2 u^L}{\partial x^2} + \frac{\partial^2 u^L}{\partial y^2} \right) = \frac{\tau_{sx}}{\rho h} - \frac{\tau_{bx}^E}{\rho h} - g \frac{\partial \eta}{\partial x} + \frac{F_x}{\rho h} \quad (4)$$

$$\frac{\partial v^L}{\partial t} + u^L \frac{\partial v^L}{\partial x} + v^L \frac{\partial v^L}{\partial y} - f u^L - v_h \left(\frac{\partial^2 v^L}{\partial x^2} + \frac{\partial^2 v^L}{\partial y^2} \right) = \frac{\tau_{sy}}{\rho h} - \frac{\tau_{by}^E}{\rho h} - g \frac{\partial \eta}{\partial y} + \frac{F_y}{\rho h} \quad (5)$$

$$\frac{\partial \eta}{\partial t} + \frac{\partial h u^L}{\partial x} + \frac{\partial h v^L}{\partial y} = 0 \quad (6)$$

135 where u^L, v^L are Lagrangian velocities, f is the Coriolis coefficient, v_h is the horizontal eddy
 136 viscosity, h is the local water depth, τ_{bx}^E, τ_{by}^E are the Eulerian bed shear stresses, η is the water
 137 level, and F_x, F_y are the radiation stress tensors (from wave action balance and roller energy
 138 balance). These equations are critical for calculating wave induced mass flux such as depth
 139 averaged undertow.

140 XBeach solves the depth-averaged 2DH advection-diffusion equation to produce transport
 141 vectors that are then used to update the bathymetry:

$$\frac{\partial hC}{\partial t} + \frac{\partial hCu^E}{\partial x} + \frac{\partial hCv^E}{\partial y} + \frac{\partial}{\partial x} \left[D_h h \frac{\partial C}{\partial x} \right] + \frac{\partial}{\partial y} \left[D_h h \frac{\partial C}{\partial y} \right] = \frac{hC_{eq} - hC}{T_s} \quad (7)$$

142 where C represents the depth-averaged sediment concentration, u^E , v^E are Eulerian mean
 143 velocities, D_d is the sediment diffusion coefficient, and T_s is a modified time scale based on
 144 sediment fall velocity and local water depth. These formulations rely on the non-hydrostatic
 145 calculation of the wave group envelope and accompanying IG waves (including bound, free and
 146 trapped long waves). Infragravity waves make a significant contribution to shoreline erosion
 147 during storms, since a large portion of the offshore suspended sediment transport occurs at IG
 148 frequencies (Masselink, 1995).

149 In (8) and (9), the equilibrium sediment concentration C_{eq} is calculated using the Soulsby-Van
 150 Rijn transport formulation (Soulsby, 1997):

$$C_{eq} = \frac{A_{sb} + A_{ss}}{h} \left(\sqrt{u_{stirring}^2} - u_{cr} \right)^{2.4} (1 - \alpha_b m) \quad (8)$$

$$u_{stirring} = \sqrt{(u^E)^2 + (v^E)^2 + 0.018 \frac{u_{rms}^2}{C_d}} \quad (9)$$

151 where A_{sb} and A_{ss} are bed and suspended load coefficients respectively, $u_{stirring}$ is the Soulsby-
 152 Van Rijn stirring velocity, u^E , v^E are Eulerian velocities, u_{rms} is the RMS bottom orbital velocity

153 from wave action (linear theory), C_d is the drag coefficient, u_{cr} is the threshold current speed
154 (from Van Rijn method) that the combined mean/infragravity and orbital short wave velocity
155 must exceed to mobilize sediment, α_b is a bed slope effect calibration factor and m is the bed
156 slope (Soulsby, 1997). Here A_{sb} and A_{ss} are functions of the median sediment grain size (D_{50}), the
157 ratio of densities of sediment grains to water, and the water depth. Furthermore, u_{cr} is a function
158 of D_{50} , the 90th percentile grain size D_{90} , and the local water depth. Wave skewness effects are
159 not incorporated into the sediment transport modeling.

160 Finally, the bed level is updated based on gradients in sediment transport rates:

$$\frac{\partial z_b}{\partial t} + \frac{f_{mor}}{(1-p)} \left(\frac{\partial q_x}{\partial x} + \frac{\partial q_y}{\partial y} \right) = 0 \quad (10)$$

161 where z_b is the bed level, f_{mor} is a morphological acceleration factor (e.g. Roelvink, 2006;
162 Ranasinghe et al., 2011), p is the sediment porosity, and q_x and q_y are sediment transport rates in
163 the cross-shore and alongshore directions respectively. The main focus of this study is on the
164 portion of a barrier island that is considered subaerial under normal conditions. The numerical
165 formulations used to simulate processes occurring during the various impact regimes are
166 described in the following.

167 The swash and collision regime both involve return flow currents (i.e. undertow and rip currents)
168 to balance the onshore mass flux created by waves, rollers, and bores. These return flows are one
169 of the main mechanisms to move sediment offshore. Since vertical variations in these return
170 flows during extreme events are limited (Roelvink et al., 2010), equations (8) and (9) are deemed

171 sufficient to deal with the complex sediment stirring mechanisms in the surf and swash zones
172 that form in the previously subaerial part of the model domain. In these storm driven surf and
173 swash zones, long-wave and mean current contributions are dominant and included in the
174 numerical formulations (e.g. van Thiel de Vries et al., 2008) in addition to short wave stirring.

175 The avalanching model employed in XBeach considers two critical slopes for dry and wet
176 portions of the beach, respectively. The critical dry slope is 1:1 and the critical wet slope is 1:3.
177 If a cell that was previously dry encounters swash runup exceeding 0.1 m inundation, its critical
178 slope is set to 1:3, effectively moving sediment into the adjacent offshore cell with a limiter on
179 actual volume transfer per time step to avoid model instability.

180 Low-frequency motions on the time-scale of wave groups are used in XBeach to model the
181 landward flux of water and sediment during the overwash regime. The momentum-conserving
182 drying/flooding formulation by Stelling and Duinmeijer (2003) is used, coupled with sediment
183 transport and bed-updating formulations as described in (8) and (10), respectively (Roelvink et
184 al., 2010).

185 During the inundation regime, XBeach employs two mechanisms to simulate dune and barrier
186 island breaching. The first is a generic formulation for sediment transport induced by breach
187 channel flow dynamics (i.e. channel flow velocities above a critical threshold value mobilize
188 sediment). In addition, breach channel bank erosion is added to the model in a similar fashion as
189 for the dune scarping/slumping process during the collision regime where wet slopes created by
190 the erosion from the breach channel flow are flattened to their critical value. It is noted that for
191 this study the ‘Groundhog Day’ release of XBeach was used (Roelvink et al., 2010).

192 **2.2. CSHORE Background**

193 CSHORE is a very efficient process-based 1D cross-shore coastal response model. The model
194 includes a time-averaged and depth-averaged combined wave and cross-shore current model, a
195 time-averaged sediment transport model, a probabilistic model for the intermittently wet and dry
196 zone, as well as empirical formulas for irregular wave runup (Johnson et al., 2012; Kobayashi et
197 al., 2008; Kobayashi, 2013). The model employs a linear wave theory based model with an
198 assumed Gaussian distribution of the free-surface elevation below mean sea level (MSL) and a
199 model based on the time-averaged continuity and momentum equations derived from nonlinear
200 shallow-water equations above still water level (SWL) to provide hydrodynamic forcing for
201 sediment transport and morphology changes. Outputs from both models are averaged in the zone
202 between SWL and MSL to provide smooth results over the entire computation domain. The
203 actual location of SWL and MSL at each time step dictates where along the profile the two
204 models are applied. CSHORE predicts cross-shore variations of the mean and standard deviation
205 of the free surface elevation, the depth-averaged cross-shore current, the cross-shore velocity
206 standard deviation, the cross-shore bed-load transport rate, and the cross-shore suspended
207 sediment transport rate. The root-mean-square wave height, spectral peak period and
208 setup/setdown with respect to SWL are used as input at the offshore boundary of the
209 computation domain. Only the initial bottom profile elevation is specified for the computation of
210 the entire model run. Since CSHORE is a 1D cross-shore time-averaged model, it is most
211 effective when applied to representative shore locations where bathymetric contours are
212 approximately parallel. Computational efficiency, robustness, and relatively good accuracy are
213 some of the major advantages of using CSHORE as a tool to predict beach profile changes.

214 The wave and current model in the wet zone is based on the time-averaged continuity and

215 momentum equations, the wave action equation, and the roller energy equation as detailed by
 216 Kobayashi (2009). In the intermittently wet and dry zone of the profile above SWL where dune
 217 scarping, overtopping, overwash, and ridge-runnel formation and migration can become
 218 important, several assumptions are made that influence how hydrodynamics, sediment transport,
 219 and morphodynamics are calculated. In the following, the most critical formulations for this zone
 220 are presented. The time-averaged cross-shore continuity and momentum equations are expressed
 221 as:

$$\overline{hU} = q_o \quad (11)$$

$$\frac{d}{dx} \left(\overline{hU^2} + \frac{g}{2} \overline{h^2} \right) = -gS_{bx}\bar{h} - \frac{1}{2}f_b\overline{|U|U} \quad ; \quad S_{bx} = \frac{dz_b}{dx} \quad (12)$$

222 where h and U are the instantaneous water depth and cross-shore velocity, respectively; q_o is the
 223 combined wave overtopping and overflow rate; g is gravitational acceleration; S_{bx} is the cross-
 224 shore bottom slope; and f_b is the bottom friction factor allowed to vary spatially.

225 All parameters are based on depth and time averages where probabilistic averaging is performed
 226 only during the time when water actually covers the respective profile location ($h>0$). An
 227 exponential probability density function of the water depth h is assumed (Kobayashi et al.,
 228 1998), allowing for the definition of a wet probability P_w as the probability of $h>0$ at any cross-
 229 shore location. The standard deviation σ_η of the free surface elevation η is given by

$$\frac{\sigma_\eta}{\bar{h}} = \left(\frac{2}{P_w} - 2 + P_w \right)^{0.5} \quad (13)$$

230

231 where \bar{h} is the mean water depth for the wet duration and $\sigma_\eta = \bar{h}$ for $P_w = 1$ (Kobayashi et al.
 232 1998). The cross-shore velocity U is assumed to be

$$U = \alpha\sqrt{gh} + U_s \quad (14)$$

233 with U_s being a steady velocity added to account for both offshore return flow on the seaward
 234 slope and the downward velocity increase on the landward slope of the profile, respectively. This
 235 formulation allows for the direct inclusion of undertow current and overtopping flow on the
 236 backside of a ridge or dune. The factor α is set to 2 based on video measurements of bore speed
 237 and flow depth over a barrier island (Holland et al. 1991), confirmed computationally by Tega
 238 and Kobayashi (1996). The steady velocity U_s is assumed zero at local maxima of the profile (i.e.
 239 ridge or dune crest).

240 The sediment transport model included in CSHORE incorporates the hydrodynamic forcing to
 241 compute depth-averaged suspended sediment load q_s and bed load q_b . In the wet and dry zone of
 242 the profile the cross-shore suspended sediment transport rate is related to the undertow current
 243 and the horizontal cross-shore velocity and is expressed as

$$q_s = (a\bar{U} + a_o U_o) V_s; \quad U_o = q_o / \bar{h} \quad (15)$$

244 where a is the suspended load parameter given by Kobayashi et al. (2009), a_o is the empirical
 245 overtopping parameter (Figlus et al. 2011), U_o is the onshore current caused by the wave
 246 overtopping rate q_o , and V_s is the suspended sediment volume per unit horizontal bottom area
 247 given by Kobayashi et al. (2009, 2010). Suspended sediment volume is related to sediment fall
 248 velocity and the energy dissipation rate due to bottom friction. In the wet and dry zone sediment
 249 transport formulations have been simplified by assuming normally incident waves and no
 250 average alongshore current.

251 The cross-shore bed load transport rate depends on the standard deviation of the depth-averaged
 252 horizontal velocity and is given by

$$q_b = \frac{b P_b \sigma_U^3}{g(s-1)} G_s \quad (16)$$

253 where b is the bedload parameter (Kobayashi et al. 2009), P_b is the probability of sediment
 254 movement (Kobayashi et al. 2008), σ_U is the standard deviation of the horizontal velocity, s is
 255 specific gravity of the sediment and G_s is the bottom slope function given by Kobayashi et al.
 256 (2008) which itself is a function of the cross-shore profile slope. Incipient mobilization of
 257 sediment is calculated using a critical Shields parameter (Ψ_c) of 0.05. The net cross-shore
 258 sediment transport rate is the sum of the net bed load and suspended sediment transport rates.

259 This model is limited to globally uniform sediment parameters characterized by the median

260 diameter (D_{50}), the fall velocity (w_f), and the specific gravity (s). The probabilistic model for the
261 wet and dry zone was calibrated and verified by the developers using small-scale lab tests and
262 limited field verification data (e.g. Kobayashi et al., 2008; Figlus et al., 2011). In general, this
263 model is used to predict wave overwash of dunes and associated morphology changes, as well as
264 structural damage progression of rubble mound coastal structures. One weakness of CSHORE is
265 that in its current state it cannot calculate offshore sediment transport due to storm surge ebb,
266 which is a major contributor to the response of FI to Hurricane Ike. However, it is expected that
267 the initial morphodynamic response to the storm can be simulated. It is noted that the 2012
268 research version of CSHORE was used for this study (Figlus et al., 2012).

269 **3. Model Setup**

270 **3.1. Boundary Conditions**

271 To ensure accurate hydrodynamic forcing conditions for the numerical models XBeach and
272 CSHORE, continuous time series of wave and water level parameters are required at or near the
273 model boundary. XBeach allows for independent hydrodynamic input to be specified at all four
274 corners of the model domain which helps ensure that time-varying water level gradients between
275 ocean and bay are represented consistently. While measured data during Hurricane Ike was
276 available in the nearshore region of FI from temporarily deployed wave buoys, no such data were
277 available inside the bay. Hence, the continuous boundary conditions were extracted from large
278 scale numerical modeling results that simulate the hydrodynamics of Hurricane Ike. For this, two
279 potential parent simulations were considered: (1) Coastal Storm Modeling System (CSTORM)
280 model results produced by the USACE Engineer Research and Development Center (ERDC),
281 and (2) ADCIRC+SWAN model results provided by Dr. Casey Dietrich of North Carolina State

282 University (Hope et al., 2013).

283 The time series of water surface elevation in the nearshore region of FI was characterized by two
284 peaks occurring roughly 11 hours apart. The first peak, which occurred on the evening of Sep-12,
285 was resultant of the forerunner surge and can be attributed to Ekman setup (Kennedy et al.,
286 2011). The second peak, which occurred on the morning of Sep-13, was resultant of the
287 hurricane storm surge. In the nearshore region, the storm surge peak was of greater magnitude
288 than the forerunner surge. Both models slightly overestimate the storm surge peak WSEL by 0.2-
289 0.4 m in the nearshore region, but underestimate the forerunner surge by up to one meter.
290 Additionally, there was a resurgence wave of smaller magnitude occurring one day after the
291 initial surge that was underestimated by about 1 m in both models. The timing of surge onset and
292 retreat is accurately captured in the nearshore environment. In the nearshore, the
293 ADCIRC+SWAN model does a slightly better job of simulating the forerunner surge, but the
294 CSTORM model more accurately predicts the peak WSEL.

295 Fig. 2 shows the validation of water surface elevation, significant wave height and peak period at
296 a nearshore location in about 8 m water depth 10 km offshore of the eastern end of FI from
297 Kennedy Gauge W (Latitude 29° 4.284', Longitude: 95° 2.375'). Further validation of modeled
298 water levels using various inshore tide gauge records in the area also show good agreement
299 (Harter, 2015). The validation of wave parameters was limited to the ADCIRC+SWAN model
300 results in this study. In the nearshore, maximum wave heights were accurately captured to within
301 0.3 m. The timing of wave onset matched recorded data, however the time of maximum wave
302 height lagged behind observations by approximately 15 hours.

303 In summary, both models are able to accurately capture maximum wave and water level

304 conditions. However, significant wave heights and water levels tend to lag by 12-15 hours. In the
305 absence of a better alternative, either one of these models are acceptable for providing boundary
306 conditions to the coastal response models, especially since the time lag was relatively consistent
307 for both water surface and wave parameters. Since simulation results from both models were
308 fairly consistent, the ADCIRC+SWAN simulation was chosen as the parent model because these
309 data were more accessible than the CSTORM data.

310 **3.2. Grid Generation**

311 XBeach uses a 2D-rectilinear grid with variable grid spacing in both x- and y-directions. The
312 model grid is oriented with the positive x-direction onshore and positive y-direction alongshore,
313 with the grid origin at the lower left corner at the offshore boundary. This orientation allows the
314 variable x-resolution to efficiently resolve cross-shore features like the foredune.

315 The variable cross-shore resolution can be calculated automatically using a specified Courant
316 condition of 0.7 with the maximum offshore boundary resolution calculated based on a minimum
317 mean period and a user defined minimum dry land resolution. This method created an
318 unreasonably small cross-shore resolution in the back bay (where wave action is expected to be
319 minimal). Thus, the cross-shore resolution of the back bay was adjusted to 20 m to minimize
320 computational expense. The final cross-shore resolution varied between 20 m at the offshore and
321 back bay boundaries and 5 m at the shoreline.

322 The final grid encompassed Follet's Island in its entirety from approximately 2.5 km offshore to
323 half way through Christmas Bay (Fig. 3). The lateral extent was from the west end of Galveston
324 Island to the Freeport Jetties. This region originally had an average elevation of 2 m NAVD88.

325 CSHORE runs on 1-D cross-shore bathymetric profiles that are oriented positive shoreward with
326 the origin at the offshore boundary. These profiles were extracted along eight survey transects
327 (Fig. 4). The model domain was truncated at highway CR-257 to maintain consistency with the
328 analysis of LiDAR data. CSHORE requires that the prescribed surge level never exceeds the
329 highest bed level in the domain.

330 ***3.3. Numerical Model Setup***

331 For the XBeach simulation, time histories of water surface elevations from the parent model
332 SWAN+ADCIRC were extracted at the four corners of the model domain. Water surface
333 boundary conditions were applied at the corners of the model domain and were interpolated
334 spatially along the boundary edges. The time steps of the water surface boundary conditions
335 were also linearly interpolated onto the model time step, meaning that the input temporal
336 resolution of water surface can be large as long as it accurately resolves storm surge.

337 Time histories of parameterized significant wave height, peak wave period and mean wave
338 direction were extracted from the parent model at the offshore boundary of the XBeach grid.
339 These parameters define a JONSWAP spectral form, which is interpolated in time to the
340 computation time step. Thus, the input wave parameter time step needs to be only small enough
341 to resolve the bound long waves.

342 XBeach is a computationally intensive model, and as an option to reduce the run time, a
343 morphological acceleration (morfac) scheme was built into the code (10). This allows the
344 possibility of artificially reducing the total model time by accelerating hydrodynamic forcing and
345 compounding sediment transport rates by some factor. In other words, the morphological time
346 scale is sped up by some prescribed factor relative to the hydrodynamic time scale. Lindemer et

347 al. (2010) and McCall et al. (2010) performed sensitivity analyses of the morphological
348 acceleration parameter and concluded that for values between 1 and 20, there was less than 2%
349 difference in the resulting coastal response, despite a significant reduction in the computation
350 time. Thus, a morfac value of 10 was chosen for the base simulation. Using a morphological
351 acceleration factor is appropriate for short-term simulations of extreme events as long as the
352 accelerated water level changes do not significantly affect the hydrodynamics. Thus, for this
353 simulation where the storm surge is directed perpendicular to the coast, the use of morfac is
354 acceptable.

355 McCall (2010) determined that XBeach will tend to over predict the morphological change
356 associated with sheet flow, such as during the inundation regime. Thus, XBeach has a built-in
357 trigger to artificially limit the maximum Shields number to a constant value, with recommended
358 values between 0.8 and 1.2 which affects the stirring velocity during sheet flow:

$$u_{stirring}^2 = \min\left(u_{stirring}^2, \theta_{sf} \frac{gD_{50}\Delta}{c_f}\right) \quad (16)$$

359 where $u_{stirring}$ is the Soulsby-Van Rijn stirring velocity during sheet flow (9), θ_{sf} is the threshold
360 Shields parameter for the start of sheet flow (denoted as s_{max} in the XBeach model input), D_{50} is
361 the median sediment grain size, and Δ is the relative density of the sediment. This method
362 assumes that during sheet flow, higher velocities correspond to higher transport rates, but not to
363 higher equilibrium sediment concentrations.

364 Sensitivity testing was conducted on the s_{max} factor to test how varying this parameter affects

365 the final bed elevation. Sensitivity tests were run in 1-D cross-shore mode only. Fig. 5 compares
366 the final bed elevation with s_{max} values from 0.8 to 1.2 for the profile at Section A. A summary
367 of the eroded and accreted volumes from these results is shown in Table 1. These volumes were
368 calculated geometrically using the pre- and simulated post-storm profiles at Section A. It is clear
369 that specifying a higher maximum Shields number leads to a greater magnitude of bed level
370 change. An s_{max} value of 0.8 was chosen for the base simulation. McCall et. al. (2010) found
371 that varying s_{max} between 0.8 – 1.2, the skill and bias of XBeach remain within reasonable
372 limits of sensitivity. The use of a Shields limiter is inherently problematic, and the most recent
373 release of XBeach (Kingsday release) features other, more physics-based effects to limit erosion
374 under sheet flow conditions. Specifically, dilatancy effects have been added to avoid the use of a
375 Shields limiter (de Vet, 2014; de Vet and Lodewijk, 2015; Roelvink et al., 2015) but the main
376 challenge remaining is the proper determination of variable bed roughness across the topographic
377 feature under investigation. Future iterations of the results presented in the following will discuss
378 the specific differences between the various methods to treat sheet flow but are beyond the scope
379 of the work presented here.

380 The additional free parameters contained in XBeach which govern model numerical schemes,
381 breaker parameters, critical avalanching slopes, etc. were all left at their default values.

382 For the CSHORE model, time histories of water surface elevation, significant wave height, peak
383 wave period, and mean wave direction were extracted from the parent model SWAN+ADCIRC
384 at the offshore boundary of each profile. Wave incident angles at the offshore boundary were
385 converted relative to shore-normal. The models were run for a total model time of 96 hours
386 beginning Sep-10, 2008 15:00 GMT.

387 **4. Model Outcomes**

388 **4.1. XBeach Results**

389 By visually observing the XBeach results, it is clear that XBeach renders the expected effects
390 involved in the collision, overwash, and inundation regimes outlined by Sallenger (2000). In
391 addition to these regimes, it is clear that specifically for this test location, storm surge ebb plays a
392 large role in transporting sediment offshore, a phenomenon also recognized by Goff et al. (2010)
393 and Hayes (1967). Fig. 6 shows snapshot images from an approximately 2 km long by 1 km wide
394 portion of the model domain during the collision regime, overtopping regime, inundation regime,
395 and during storm surge ebb.

396 From hours 32 to 52, the island was in the overtopping regime, during which time the foredune
397 crest elevation was lowered slightly in some areas as wave runup washed sediment from the
398 lower elevation dunes to the back barrier. During this regime, the morphological response was
399 mostly limited to the dune and immediate back-barrier where dune overwash sediments were
400 deposited just landward of the foredune. Beach erosion during this regime was minimal.

401 From hours 52 to 62, FI experienced massive erosion of the foredune during the inundation
402 regime. In the hours leading up to landfall, the storm surge spiked rapidly and the foredune,
403 which had already been lowered slightly during the overwash regime, was uniformly inundated
404 causing a large volume of sediment to be transported from the foredune to the back barrier and
405 back bay. During this regime, wave action was minimal and the sheet flow from the surge
406 gradient dominated the sediment transport process.

407 From hours 62 to 73, high velocities from the ebbing storm surge pulled large volumes of

408 sediment offshore, further flattening and lowering the beach and steepening the subaqueous
409 shoreface. After the storm surge ebb, the island experienced a resurgence wave; however this
410 wave was not large enough to overtop the island a second time. This resurgence wave had
411 minimal impact on the shoreface, but did raise the forebeach elevation slightly.

412 Fig. 7 outlines each impact regime and the associated hydrodynamics and morphological
413 response based on the XBeach model runs. The cumulative volume changes associated with each
414 impact regime and the respective hourly rates of accretion and erosion are shown in Table 2 in
415 addition to the volume changes estimated from LiDAR measurements made in April, 2006
416 before Hurricane Ike and December, 2008 just after Hurricane Ike. The accreted and eroded
417 volumes were calculated by subtracting the original topography from the topography at the end
418 of each regime and identifying all positive values as accretion and all negative values as erosion.
419 The accretion and erosion rates were calculated by dividing the difference in the accreted and
420 eroded volumes between each regime by the duration of that regime.

421 It is clear from this table that the total accreted and eroded sediment volume increased by nearly
422 60% during the 10 hour inundation regime where the rates of accretion and erosion both
423 approximately doubled compared to the collision or overwash regimes. During the 11 hours
424 storm surge ebb regime, the rate of erosion was about 54% and the rate of accretion was about
425 71% of their respective rates during the inundation regime, but still at least 50% higher than
426 during the other regimes. While the rate of accretion and erosion had similar magnitudes during
427 the inundation regime, the rate of erosion was 4,176 m³/hr larger than the rate of accretion during
428 the surge ebb regime indicating this regime's significance in offshore sediment transport.
429 Additionally, to observe the cross-shore morphological response during each impact regime,
430 Table 3 summarizes the volume accreted and eroded at the end of each regime for Section D as

431 an example.

432 Simulated post-storm bed level profiles were compared with post-storm LiDAR profiles along
433 the cross-shore transects shown in Fig. 4. Sample profiles from Section A and Section D are
434 shown in Fig. 8. It is clear from this figure that the overwash regime had a much more significant
435 impact on Section A than on Section D. This is likely due to the fact that the initial dune crest
436 elevation at Section A was approximately 50 cm lower than at Section D. Furthermore, due to
437 the lower elevation on the east end of the island, the resurgence wave had a relatively greater
438 impact on Section A than any of the other sections. Here the shoreline was extended farther
439 offshore between hours 73 and 96, where the other areas experienced little impact.

440 The XBeach simulation was able to capture the large scale 2D erosional patterns of the island.
441 The locations of two significant breaches were accurately reproduced with XBeach (Fig. 9). Both
442 of these locations initially had a relatively low and narrow foredune, and thus were particularly
443 susceptible to breaching. Although the large-scale erosion trends are accurately simulated in
444 XBeach, it is clear that the small-scale erosion patterns (such as the specific storm surge ebb
445 channels) are not accurately reproduced (Fig. 9). This is likely due to the simplifications and
446 assumptions inherent to the model formulations and, probably to a lesser degree, to the influence
447 of structures, vegetation, and spatially variable geology that are not included in the XBeach
448 model.

449 One way to quantify the accuracy of a model is to compare the error in modeled bed level change
450 to the variance of the observed bed level change from LiDAR data; known as the simulation
451 skill (17). It is also important to calculate the mean error in the simulation to determine whether
452 the simulation errors are due to random differences in bed elevation or due to a general trend;

453 known as the simulation bias (18). Since these values can only be computed in areas where data
 454 sources overlap, the calculations are limited to the subaerial beach where LiDAR surveys are
 455 available (McCall et al., 2010).

$$Skill = 1 - \frac{\sum_{i=1}^N (dz_{b_{LIDAR,i}} - dz_{b_{Model,i}})^2}{\sum_{i=1}^N (dz_{b_{LIDAR,i}})^2} \quad (17)$$

$$Bias = \frac{1}{N} \sum_{i=1}^N (z_{b_{post-storm,Model,i}} - z_{b_{post-storm,LIDAR,i}}) \quad (18)$$

456 where N is the total number of grid points in the overlapping coverage area, $dz_{b_{LIDAR,i}}$ is the
 457 measured bed level change at point i , and $dz_{b_{Model,i}}$ is the modeled bed level change at point i .

458 If the skill is equal to one, then the simulation perfectly predicts the bed level change. If the skill
 459 is zero, then the simulation is no more accurate than predicting zero bed level change. If the skill
 460 is less than zero, then the simulation is less accurate than predicting zero bed level change.
 461 Furthermore, a positive bias means the model has predicted a higher post-storm bed elevation
 462 than is observed, and a negative bias means the model has predicted a lower post-storm bed
 463 elevation.

464 Based on (17) and (18) the skill of this XBeach simulation is 0.35 with an overall bias of -0.06.
 465 This is considerably lower than the skill of 0.74 from a similar study by McCall et al. (2010).
 466 There are a number of factors that could contribute to this. Where the study by McCall et al.
 467 focused on a mostly unvegetated stretch of island, the back barrier of Follet's Island is
 468 abundantly covered with grass, which cannot be included in the current build of XBeach. De Vet
 469 et al. (2015) attempted to include the effects of vegetation on coastal response with some success

470 by using a spatially variable Manning's roughness coefficient. However, this method still
471 requires some testing to confirm its accuracy at modeling the impact of vegetation. In addition to
472 the influence of vegetation, there are likely errors in the computed difference in the LiDAR
473 surveys from the filtering of buildings and foliage, which was performed by deleting any areas
474 that showed a net gain in land surface that exceeded two meters; the assumption being that a
475 greater than two meter net rise in bed level is unrealistic and thus represents the existence of
476 buildings or foliage.

477 The skill of this simulation is shown graphically in Fig. 10, where the measured bed level change
478 is plotted relative to the modeled bed level change. The color scale in this plot represents the
479 point density in points per square meter. It is clear from Fig. 10 that the greatest density of
480 measured bed change was between -5 cm and +30 cm. Based on this figure, XBeach had a
481 tendency to underestimate both accretional and erosional bed level change. There is also a cluster
482 of points of measured bed level change greater than 1 m that were significantly underestimated
483 by XBeach. It is likely that these points are associated with the difference in LiDAR returns
484 between the pre- and post-Ike surveys that were not filtered out.

485 ***4.2. CSHORE Results***

486 CSHORE was run separately for the eight different bed profiles associated with Sections A-H
487 (Fig. 4). During the collision regime, the foredune, beach, and foreshore experienced only
488 minimal bed level change. During the overwash regime, the wave runup exceeded the dune crest
489 causing washover of dune sediments and slight lowering of the dune crest (0.1 – 0.6 m). During
490 the inundation regime, the beach was flattened and the shoreline extended seaward while the
491 dune was drastically lowered in elevation and pushed landward. There was very little bed level

492 change associated with storm surge ebb and the resurgence wave since CSHORE does not model
493 offshore directed return flow in its current build and the resurgence wave was not large enough
494 to cause major morphological changes.

495 Table 4 summarizes the volume accreted and eroded at the end of each regime for Section D as
496 an example. The bulk of the bed level change was associated with the overwash and inundation
497 regimes. Erosion rates during the inundation regime were still higher than any other regime, but
498 not proportionally as high as in the XBeach model. Also unlike the XBeach model, the storm
499 surge ebb regime did not have a significant impact on the total bed level change. This is
500 understandable as the hydrodynamics associated with the ebbing storm surge are not built into
501 the time-averaged CSHORE model.

502 Simulated post-storm bed level profiles were compared with post-storm LiDAR profiles along
503 Sections A-H (Fig. 4). Sample profiles from Section A and Section D are shown in Fig. 11.
504 Based on these figures it is clear that CSHORE very accurately predicted the post-storm beach
505 slope and shoreline. However, CSHORE was less effective at predicting the morphology of the
506 foredune. This is likely due to the fact that the dune morphodynamics are largely driven by sheet
507 flow associated with inundation; a physical process that is not explicitly included in the
508 CSHORE model.

509 The skill and bias of the CSHORE simulations were calculated for each profile and these values
510 are summarized in Table 4. Since Sections F-H are located on the more developed west end of
511 the island, it is likely that anthropogenic influences contribute to the lower skill for these
512 sections. Excluding Sections F-H, the skill becomes 0.408 and the bias 0.737. Sections B and C
513 display a clear positive bias that is likely due to truncation of the domain at CR-257.

514 To compare the skill of CSHORE directly with that of XBeach, the skill of each model must be
515 calculated over the same coverage area. Since the CSHORE calculation is limited to cross-shore
516 transects, the skill and bias of XBeach on those same transects were calculated and shown in
517 Table 4 for direct comparison with CSHORE results.

518 The total skill of the CSHORE simulations was 0.35, approximately the same as the total skill of
519 the XBeach simulation. However, when evaluating the skill only on cross-shore Sections A-E the
520 skill of CSHORE was approximately 30% lower than Xbeach. In fact, on the east end of the
521 island (Sections A & B), XBeach showed skill as high as 0.81. However, near the center and
522 west end of the island, CSHORE had a higher skill than XBeach. This is likely due to the fact
523 that the resilient vegetation in that region prevented the dune from being completely eroded.
524 Thus, the fact that CSHORE inherently underpredicts the lowering of the dune during the
525 inundation regime coincidentally results in a better skill score at Sections D-F.

526 **5. Discussion and Conclusions**

527 In this study, the morphodynamics of the subaerial portion of Follet's Island (FI), a low-lying,
528 sediment-starved barrier island on the Upper Texas Coast (UTC), were examined in response to
529 hydrodynamic forcing conditions from Hurricane Ike. Hurricane Ike was one of the most
530 destructive storms to ever hit the UTC. Although FI was on the western side of Ike's eye at
531 landfall and thus subject to predominantly offshore directed winds, the resulting storm surge
532 overtopped and inundated the island. During this process, complex hydrodynamic forcing
533 associated with ocean-to-bay directed overwash sheet flow and subsequent bay-to-ocean directed
534 storm surge ebb sheet flow modified the morphology of FI drastically.

535 The description and quantification of the impact dynamics and regimes during the storm are

536 purely based on the presented model simulations and have to be interpreted as such. In the
537 XBeach model, the inundation regime came on extremely rapidly, effectively inundating the
538 entire length of the island simultaneously and leveling the dune across the entire length of the
539 island. The return flow of the storm surge was the same, occurring so rapidly that it was almost
540 uniform over the island length resulting in a large number of small erosion channels located
541 along the foredune and beach face region where most of the freshly reworked sediment resided
542 (evident in Fig. 9). Despite the fairly uniform inundation and storm surge ebb hydrodynamics,
543 and despite the relatively consistent maximum crest elevation along the island (only
544 approximately 0.4 m difference), several localized preferential flow areas were reactivated by the
545 hurricane and were modeled very accurately by XBeach (see Fig. 9). These larger scale breaches
546 are visible in both the model results and aerial imagery and have been identified as historic
547 breach locations.

548 The inundation and storm surge ebb regimes contributed significantly to morphological changes
549 of FI. Thus, sheet flow is thought to have an important influence, as well as specific variable bed
550 roughness over the entire island. The version of XBeach used in this study (Groundhog Day
551 release) employs a Shields limiter approach to control the effects of sheet flow on
552 morphodynamic changes as discussed in sections 2.1. and 3.3, respectively. Variable bed
553 roughness across the island (due to varying vegetation, sediment composition, and/or
554 infrastructure) have not been incorporated into the present study since the underlying data set did
555 not provide that level of detail. For example second return LiDAR information that could be used
556 to infer vegetation coverage and elevation was not available. Current research efforts related to
557 this and new data sets are ongoing and include an investigation to determine potential
558 modifications to the presented findings based on the use of the most recent XBeach version

559 (Kingsday release). Initial comparisons do not indicate significant changes to our presented
560 findings but a more detailed comparison is envisioned in a future manuscript. Based on the
561 numerical modeling results, it is clear that both XBeach and CSHORE were able to reproduce
562 the morphological response of FI to Hurricane Ike with varying degrees of skill. XBeach was
563 more accurate at simulating the coastal response to the foredune and beach system, and was also
564 able to capture 2D effects such as the locations of large breaches. It includes model routines for
565 calculating hydrodynamics and transport due to sheet flow; something that proved to be a major
566 contributor to the overall response of the island. However, XBeach required a significantly
567 longer run time than CSHORE, making it a less practical model choice for simulating large
568 numbers of storms or design scenarios in future coastal projects.

569 CSHORE was able to accurately calculate the post-storm slope and shoreline, however was less
570 effective at simulating the response of the foredune. Furthermore, it does not include routines for
571 sheet flow, making it an impractical model choice for scenarios where sheet flow is likely to be a
572 major driver of the coastal response. CSHORE has further limitations on the model domain. In
573 its current build, CSHORE is unable to simulate transport across a full cross-section of the
574 island, from offshore to the back bay, and cannot capture 2D alongshore transport trends. Despite
575 these limitations, CSHORE was able to simulate the response of individual FI cross-shore
576 profiles with a skill as high as 0.61.

577 Both models show that the greatest change in bed level of FI was associated with the inundation
578 regime of Hurricane Ike, which lasted only about 10 hours. During this regime, bed level change
579 rates were up to three times greater than during the collision and overwash regimes. XBeach was
580 also able to capture significant bed level change associated with storm surge ebb which
581 corresponds with observations of multiple ebb flow channels that were scarped into the island

582 after the passage of Hurricane Ike. This case study stresses the fact that the behavior of barrier
583 islands during storm impact is a highly dynamic and complex process and that continued
584 research into the morphodynamics of barrier islands is necessary to better understand how these
585 valuable natural and economic assets behave during extreme events.

586 **Acknowledgements**

587 This project was supported in part by an Institutional Grant (NA14OAR4170102) to the Texas
588 Sea Grant College Program from the National Sea Grant Office, National Oceanic and
589 Atmospheric Administration, U.S. Department of Commerce. Additional funding was provided
590 by the Texas General Land Office and NOAA through the Texas Coastal Management Program,
591 Grant number 13-431-000-7890. Support during the data mining process was also provided by
592 the Texas General Land Office and Coast & Harbor Engineering, a Division of Hatch-Mott
593 McDonald. The authors would like to thank Dr. Casey Dietrich and Dr. Andrew Kennedy for
594 providing the ADCIRC+SWAN model outputs used as the forcing conditions in this study and
595 the measured gauge data during Hurricane Ike, respectively.

596 **References**

- 597 de Vet, P. L. M. (2014). *Modelling sediment transport and morphology during overwash and*
598 *breaching events* (M.Sc. Thesis). TU Delft, Delft University of Technology.
- 599 de Vet, P., & Lodewijk, M. (2015). Modelling dune erosion, overwash and breaching at Fire
600 Island (NY) during Hurricane Sandy. *Proceedings of Coastal Sediments 2015, San Diego,*
601 *CA.*

602 de Vries, J. V. T., Van Gent, M. R. A., Walstra, D. J. R., & Reniers, A. J. H. M. (2008). Analysis
603 of dune erosion processes in large-scale flume experiments. *Coastal Engineering*, 55(12),
604 1028-1040.

605 Figlus, J., Kobayashi, N., & Gralher, C. (2012). Onshore migration of emerged ridge and ponded
606 runnel. *Journal of Waterway, Port, Coastal, and Ocean Engineering*, 138(5), 331–338.

607 Figlus, J., Kobayashi, N., Gralher, C., & Iranzo, V. (2011). Wave Overtopping and Overwash of
608 Dunes. *Journal of Waterway, Port, Coastal, and Ocean Engineering*, 137(1), 26–33.

609 Goff, J. A., Allison, M. A., & Gulick, S. P. S. (2010). Offshore transport of sediment during
610 cyclonic storms: Hurricane Ike (2008), Texas Gulf Coast, USA. *Geology*, 38(4), 351–354.

611 Harter, C. F. (2015). *The impact of Hurricane Ike on the geomorphology of Follet's Island,*
612 *Texas - Short and Long Term Effects* (M.Sc. Thesis). Texas A&M University, College
613 Station.

614 Hayes, M. O. (1967). Hurricanes as Geological Agents, South Texas Coast: Geological Notes.
615 *AAPG Bulletin*, 51(6), 937–942.

616 Holland, K. T., Holman, R. A., & Sallenger, A. H. (1991). Estimation of overwash bore
617 velocities using video techniques. In *Proceedings Coastal Sediments* (pp. 489–497). ASCE.

618 Hope, M. E., Westerink, J. J., Kennedy, A. B., Kerr, P. C., Dietrich, J. C., Dawson, C., ...
619 Westerink, L. G. (2013). Hindcast and validation of Hurricane Ike (2008) waves, forerunner,
620 and storm surge. *Journal of Geophysical Research: Oceans*, 118(9), 4424–4460.

- 621 Houser, C., Hapke, C., & Hamilton, S. (2008). Controls on coastal dune morphology, shoreline
622 erosion and barrier island response to extreme storms. *Geomorphology*, *100*, 223–240.
- 623 Johnson, B. D., Kobayashi, N., & Gravens, M. B. (2012). *Cross-Shore numerical model*
624 *CSHORE for waves, currents, sediment transport and beach profile evolution* (Technical
625 Report No. ERDC/CHL-TR-12-22). Vicksburg, MS: Engineer Research and Development
626 Center.
- 627 Kennedy, A. B., Gravois, U., Zachry, B. C., Westerink, J. J., Hope, M. E., Dietrich, J. C., ...
628 Dean, R. G. (2011). Origin of the Hurricane Ike forerunner surge: HURRICANE IKE
629 FORERUNNER. *Geophysical Research Letters*, *38*(8), 1–5.
- 630 Kobayashi, N. (2013). *Cross-shore numerical model CSHORE 2013 for sand beaches and*
631 *coastal structures* (Research Report No. CACR-13-01). Newark, DE: University of
632 Delaware.
- 633 Kobayashi, N., Buck, M., Payo, A., & Johnson, B. D. (2009). Berm and dune erosion during a
634 storm. *Journal of Waterway, Port, Coastal, and Ocean Engineering*, *135*(1), 1–10.
- 635 Kobayashi, N., de los Santos, F. J., & Kearney, P. G. (2008). Time-averaged probabilistic model
636 for irregular wave runup on permeable slopes. *Journal of Waterway, Port, Coastal, and*
637 *Ocean Engineering*, *134*(2), 88–96.
- 638 Kobayashi, N., Farhadzadeh, A., Melby, J., Johnson, B., & Gravens, M. (2010). Wave
639 Overtopping of Levees and Overwash of Dunes. *Journal of Coastal Research*, *265*, 888–900.
640 <https://doi.org/10.2112/JCOASTRES-D-09-00034.1>

641 Kobayashi, N., Herrman, M. N., Johnson, B. D., & Orzech, M. D. (1998). Probability
642 distribution of surface elevation in surf and swash zones. *Journal of Waterway, Port,
643 Coastal, and Ocean Engineering*, 124(3), 99–107.

644 Leatherman, S. P., Rampino, M. R., & Sanders, J. E. (1983). Barrier island evolution in response
645 to sea level rise; discussion and reply. *Journal of Sedimentary Research*, 53(3), 1026–1033.

646 Lennon, G. (1991). The nature and causes of hurricane-induced ebb scour channels on a
647 developed shoreline. *Journal of Coastal Research*, 237–248.

648 Lindemer, C. A., Plant, N. G., Puleo, J. A., Thompson, D. M., & Wamsley, T. V. (2010).
649 Numerical simulation of a low-lying barrier island's morphological response to Hurricane
650 Katrina. *Coastal Engineering*, 57(11–12), 985–995.

651 Mason, C. (1981). *Hydraulics and Stability of Five Texas Inlets* (Report No. 81–1) (p. 109). Fort
652 Belvoir, VA: U.S. Army Corps of Engineers Coastal Engineering Research Center.

653 Masselink, G. (1995). Group bound long waves as a source of infragravity energy in the surf
654 zone. *Continental Shelf Research*, 15(13), 1525–1547.

655 McCall, R. T., Van Thiel de Vries, J. S. M., Plant, N. G., Van Dongeren, A. R., Roelvink, J. A.,
656 Thompson, D. M., & Reniers, A. J. H. M. (2010). Two-dimensional time dependent
657 hurricane overwash and erosion modeling at Santa Rosa Island. *Coastal Engineering*, 57(7),
658 668–683.

659 Morton, R. A., Paine, J. G., & Gibeaut, J. C. (1994). Stages and durations of post-storm beach
660 recovery, southeastern Texas coast, USA. *Journal of Coastal Research*, 884–908.

- 661 Morton, R. A., & Pieper, M. J. (1975). *Shoreline changes in the vicinity of the Brazos river delta*
662 *(San Luis Pass to Brown Cedar Cut) - An analysis of historical changes of the Texas Gulf*
663 *shoreline* (Geological Circular No. 75-4) (p. 50). Austin, TX: Texas Bureau of Economic
664 Geology.
- 665 Morton, R. A., & Sallenger Jr., A. H. (2003). Morphological impacts of extreme storms on sandy
666 beaches and barriers. *Journal of Coastal Research*, 19(3), 560-573.
- 667 Paine, J. G., Mathew, S., & Caudle, T. (2012). Historical shoreline change through 2007, Texas
668 Gulf Coast: rates, contributing causes, and Holocene context. *Gulf Coast Association of*
669 *Geological Societies Journal*, 1, 13-26.
- 670 Ranasinghe, R., Swinkels, C., Luijendijk, A., Roelvink, D., Bosboom, J., Stive, M., & Walstra,
671 D. (2011). Morphodynamic upscaling with the MORFAC approach: Dependencies and
672 sensitivities. *Coastal Engineering*, 58(8), 806-811.
- 673 Roelvink, D., Reniers, A., Ap van Dongeren, J. van T., de Vries, J. L., & McCall, R. (2010).
674 *XBeach Model Description and Manual - v6* (p. 108). Delft, The Netherlands: Deltares.
- 675 Roelvink, D., Reniers, A., van Dongeren, A., van Thiel de Vries, J., McCall, R., & Lescinski, J.
676 (2009). Modelling storm impacts on beaches, dunes and barrier islands. *Coastal Engineering*,
677 56(11-12), 1133-1152.
- 678 Roelvink, D., Van Dongeren, A., McCall, R. T., & Hoonhout, B. (2015). *XBeach Technical*
679 *Reference: Kingsday Release - Model description and reference guide to functionalities* (p.
680 141). Delft, The Netherlands: Deltares.

- 681 Roelvink, J. A. (2006). Coastal morphodynamic evolution techniques. *Coastal Engineering*,
682 53(2–3), 277–287.
- 683 Rosati, J. D., & Stone, G. W. (2009). Geomorphologic evolution of barrier islands along the
684 northern U.S. Gulf of Mexico and implications for engineering design in barrier restoration.
685 *Journal of Coastal Research*, 25(1), 8–22.
- 686 Sallenger Jr, A. H. (2000). Storm impact scale for barrier islands. *Journal of Coastal Research*,
687 16(3), 890–895.
- 688 Sherwood, C. R., Long, J. W., Dickhudt, P. J., Dalyander, P. S., Thompson, D. M., & Plant, N.
689 G. (2014). Inundation of a barrier island (Chandeleur Islands, Louisiana, USA) during a
690 hurricane: Observed water-level gradients and modeled seaward sand transport: Barrier-
691 island inundation. *Journal of Geophysical Research: Earth Surface*, 119(7), 1498–1515.
- 692 Soulsby, R. (1997). *Dynamics of Marine Sands: A Manual for Practical Applications*. Thomas
693 Telford, London.
- 694 Stelling, G. S., & Duijnmeijer, S. A. (2003). A staggered conservative scheme for every Froude
695 number in rapidly varied shallow water flows. *International Journal for Numerical Methods*
696 *in Fluids*, 43(12), 1329–1354.
- 697 Tedesco, L. P., Wanless, H. R., Scusa, L. A., Risi, A. J., & Gelsanliter, S. (1995). Impact of
698 Hurricane Andrew on South Florida's Sandy Coastlines. *Journal of Coastal Research*, (21),
699 59–82.

700 Tega, Y., & Kobayashi, N. (1996). Wave overwash of subaerial dunes. *Coastal Engineering*
701 *Proceedings*, 1(25), 4148–4160.

702 Thieler, E. R., & Bush, D. M. (1991). Hurricanes Gilbert and Hugo send powerful messages for
703 coastal development. *Journal of Geological Education*, 39, 291–298.

704 Wang, P., Kirby, J. H., Haber, J. D., Horwitz, M. H., Knorr, P. O., & Krock, J. R. (2006).
705 Morphological and Sedimentological Impacts of Hurricane Ivan and Immediate Poststorm
706 Beach Recovery along the Northwestern Florida Barrier-Island Coasts. *Journal of Coastal*
707 *Research*, 1382–1402.

708 Zhang, K., Douglas, B., & Leatherman, S. (2002). Do Storms Cause Long-Term Beach Erosion
709 along the U.S. East Barrier Coast? *Geology*, 110(4), 493–502.

710

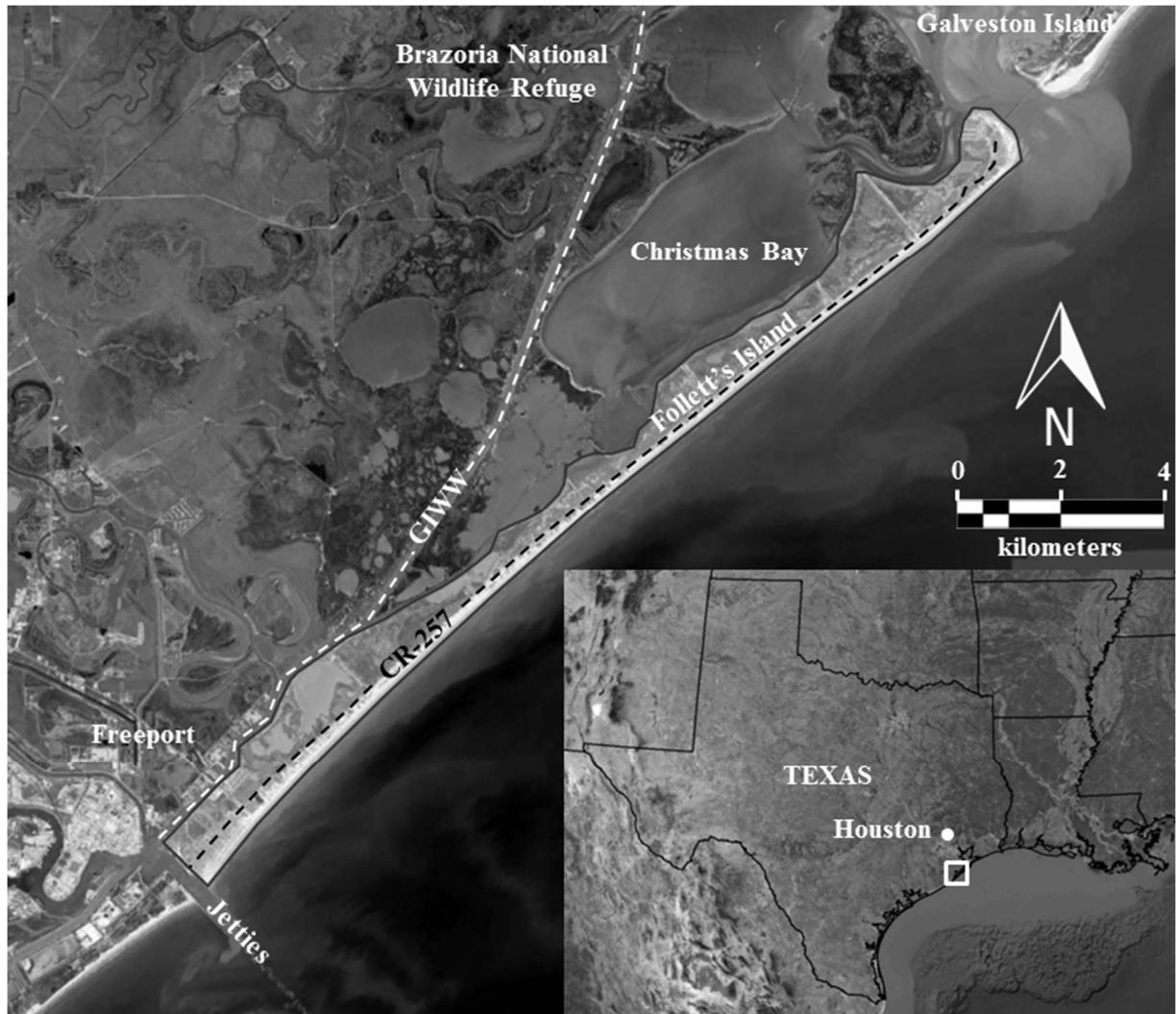


Fig. 1. Follett's Island area map showing important economic assets such as the Port of Freeport, the Gulf Intracoastal Waterway (GIWW), and the CR-257 highway as well as ecological assets like Christmas Bay and the Brazoria National Wildlife Refuge.

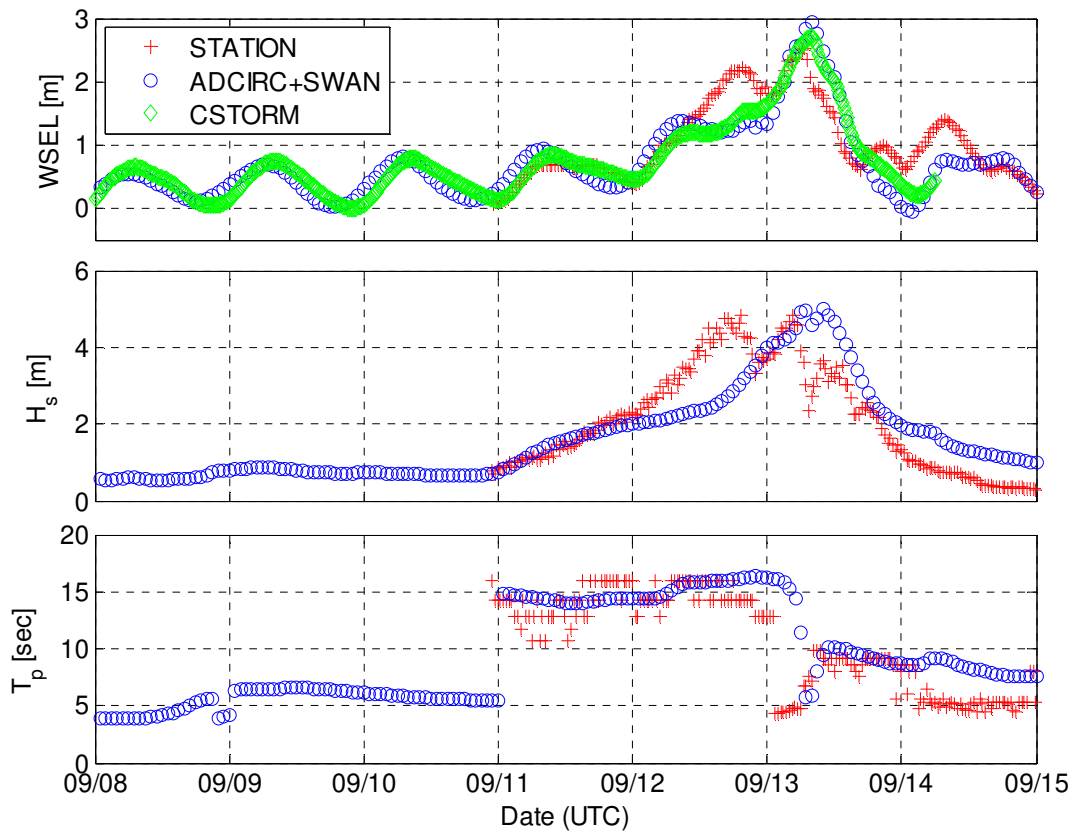


Fig. 2: Validation of modeled WSEL (top), H_s (middle) and T_p (bottom) at nearshore location: Kennedy Gauge W.

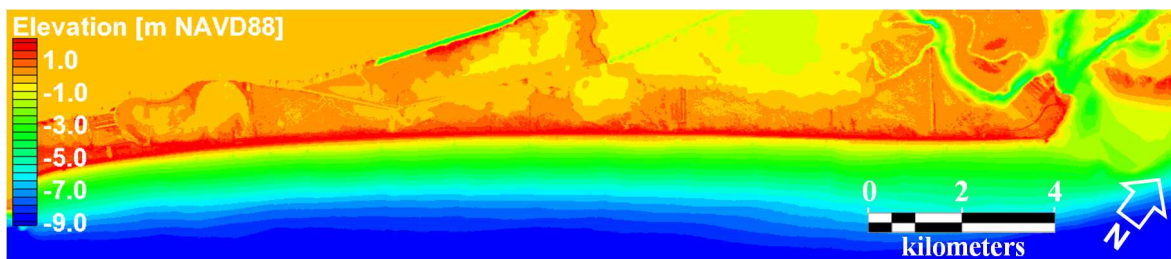


Fig. 3: Bounds and relief of the XBeach model grid.

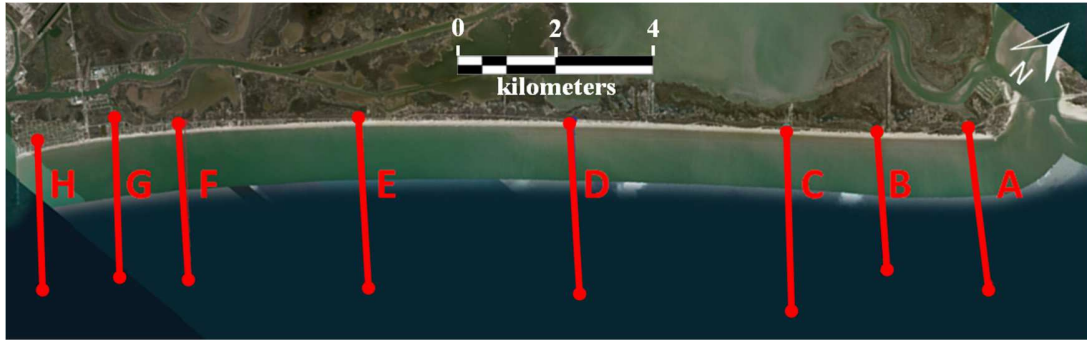


Fig. 4: Cross-shore transects for analysis of island topography and bathymetry.

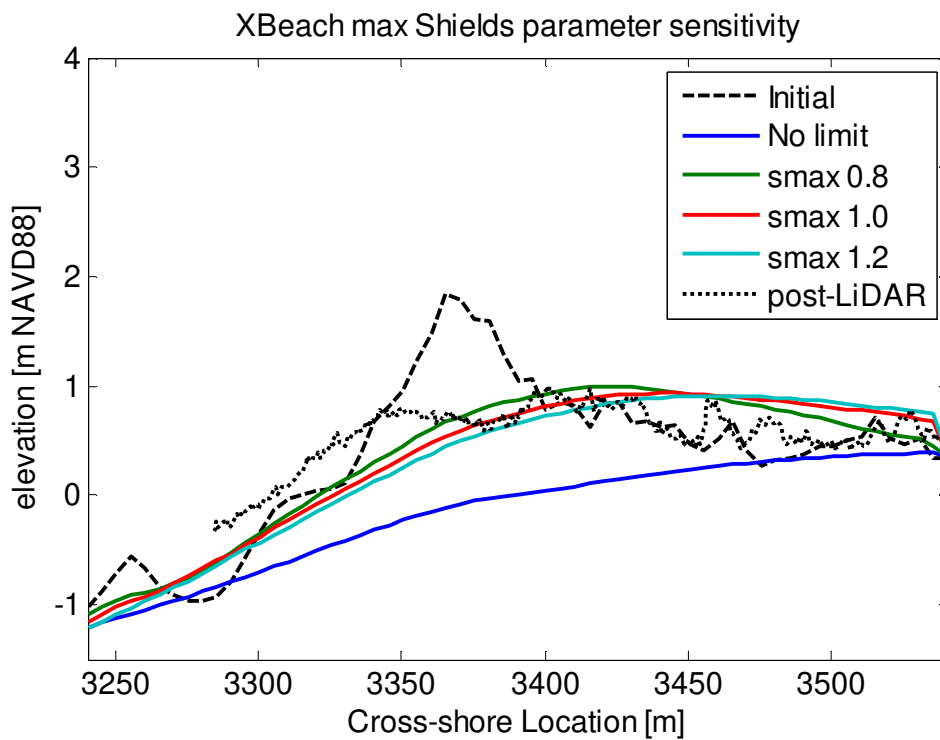


Fig. 5: Final land surface elevation comparison from XBeach model with varying s_{max} values.

This simulation was run in 1-D mode on cross-shore Section A.

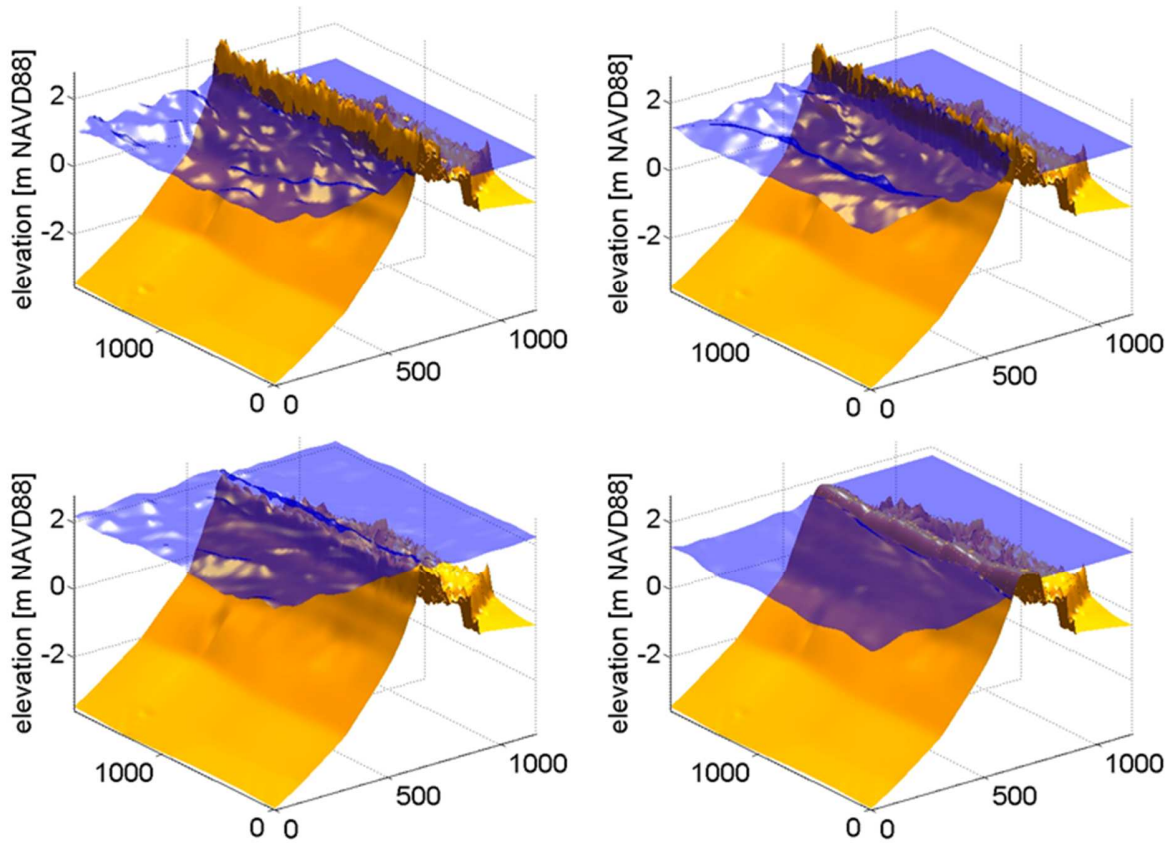


Fig. 6: Snapshot of water surface (long waves only) and bed level during the collision regime (top-left), during the overtopping regime (top-right), during the inundation regime (bottom-left), and during storm surge ebb (bottom-right).

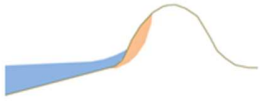

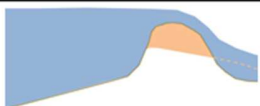
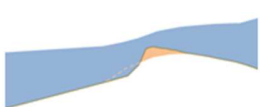

	Time [hrs]	Hydrodynamic characteristics	Morphological Response	Schematic
Collision	0 - 32	Wave runup attacks the dune face.	Sediments from the dune toe and dune face are pulled offshore.	
Overwash	32-52	Wave runup level exceeds the dune crest.	Sediments from the dune crest are washed over to the back barrier.	
Inundation	52-62	Surge level exceeds the dune crest.	Significant washover of dune sediments to the back barrier.	
Ebb	62-73	Storm surge recedes and flows back to the ocean	Sediment is dragged back offshore creating scour channels.	
End	73-96	Surge has completely receded and waves dominate the hydrodynamics	Minimal morphological response	

Fig. 7: Outline of Hurricane Ike storm impact regimes on Follet's Island based on numerical modelling results.

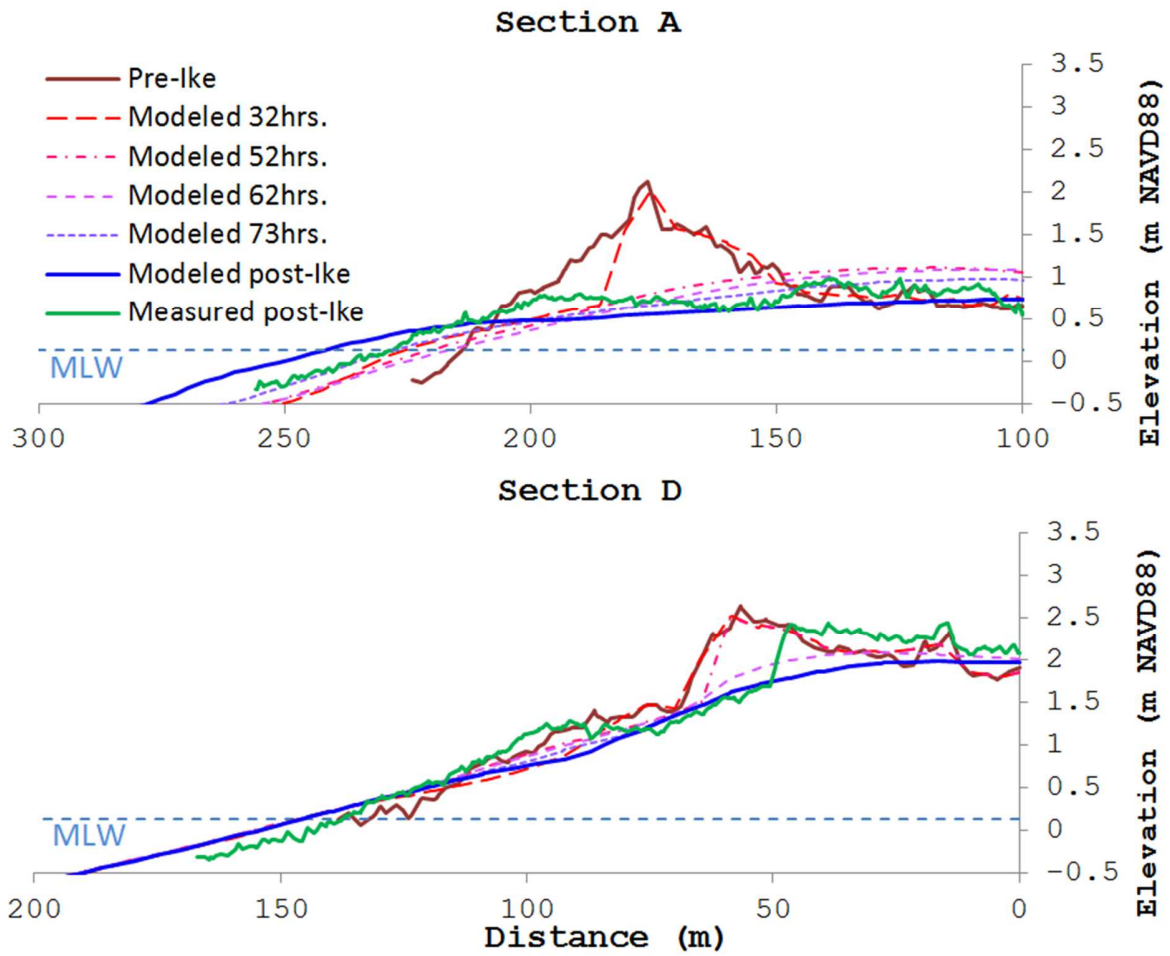


Fig. 8: XBeach simulated bed level evolution compared to pre- and post-storm bed level extracted from LiDAR data at Sections A (the east end of FI) and Section D (near the center of FI).

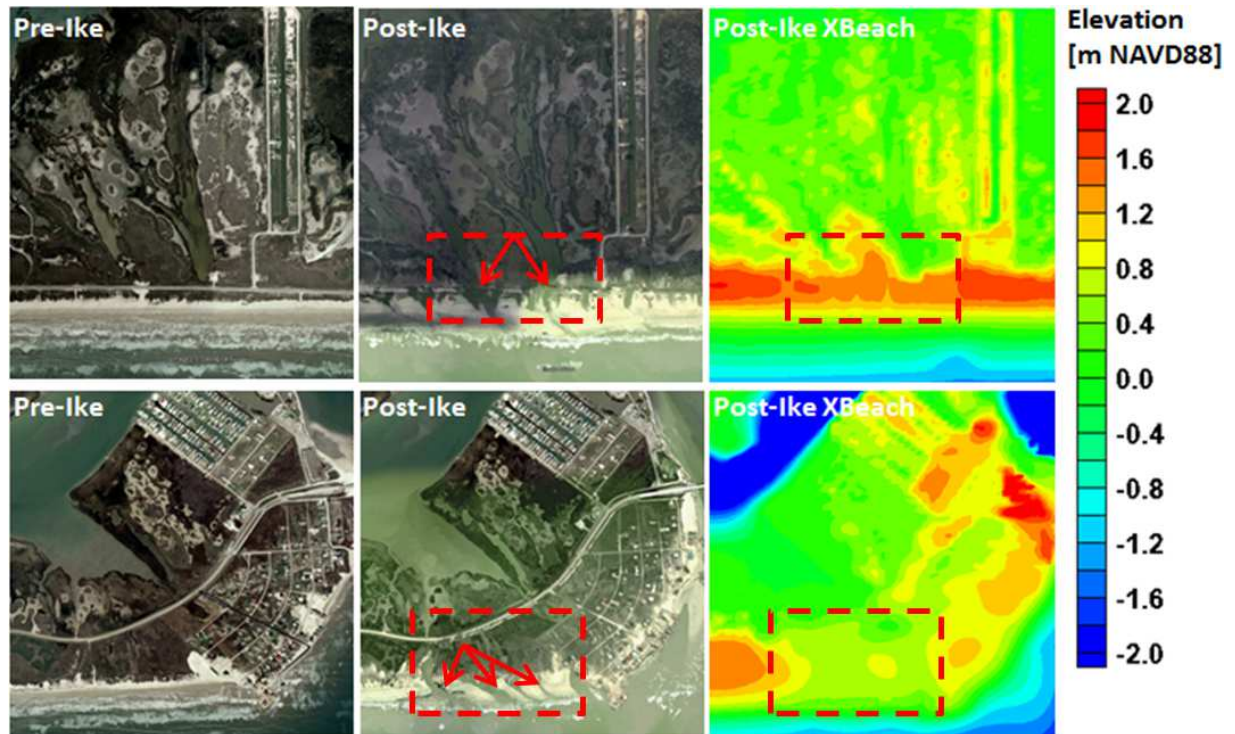


Fig. 9: XBeach simulated erosion trends compared with aerial photography observations for a middle section (top panels) and the eastern end (bottom panels) of FI. Boxed areas represent large scale 2D erosional patterns. Arrows identify smaller scale storm surge ebb channels.

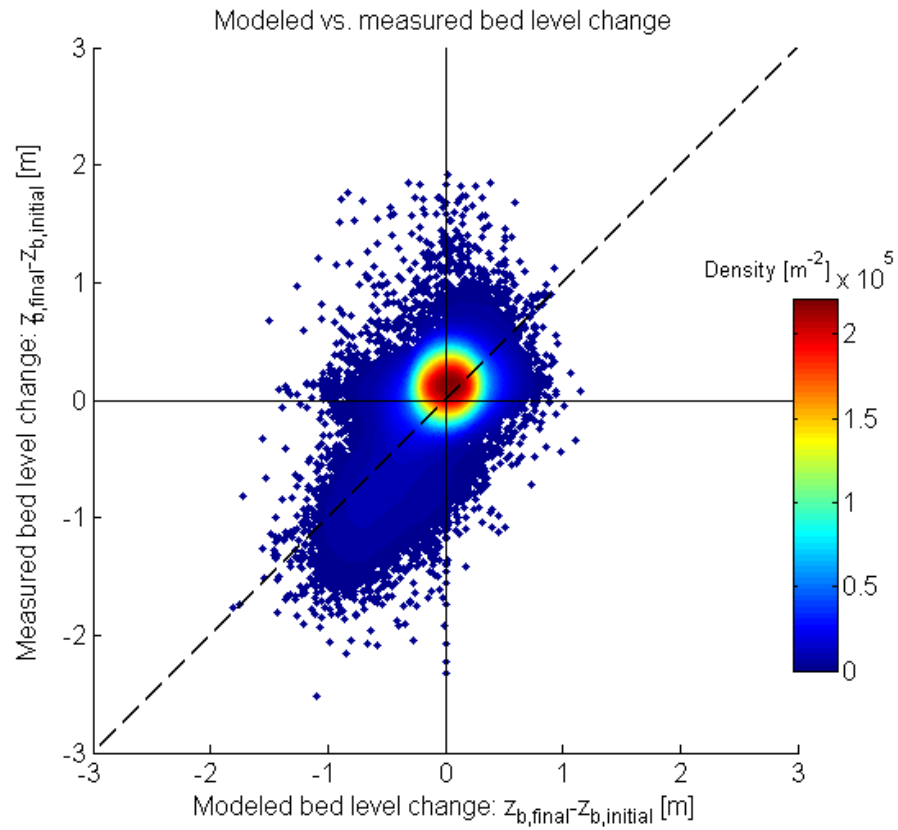


Fig. 10: Measured bed level change vs. modeled bed level change for all grid points in overlapping coverage area. The dashed line represents a perfect 1:1 relation. Color scale indicates point density in points per square meter. Positive values represent accretion and negative values represent erosion.

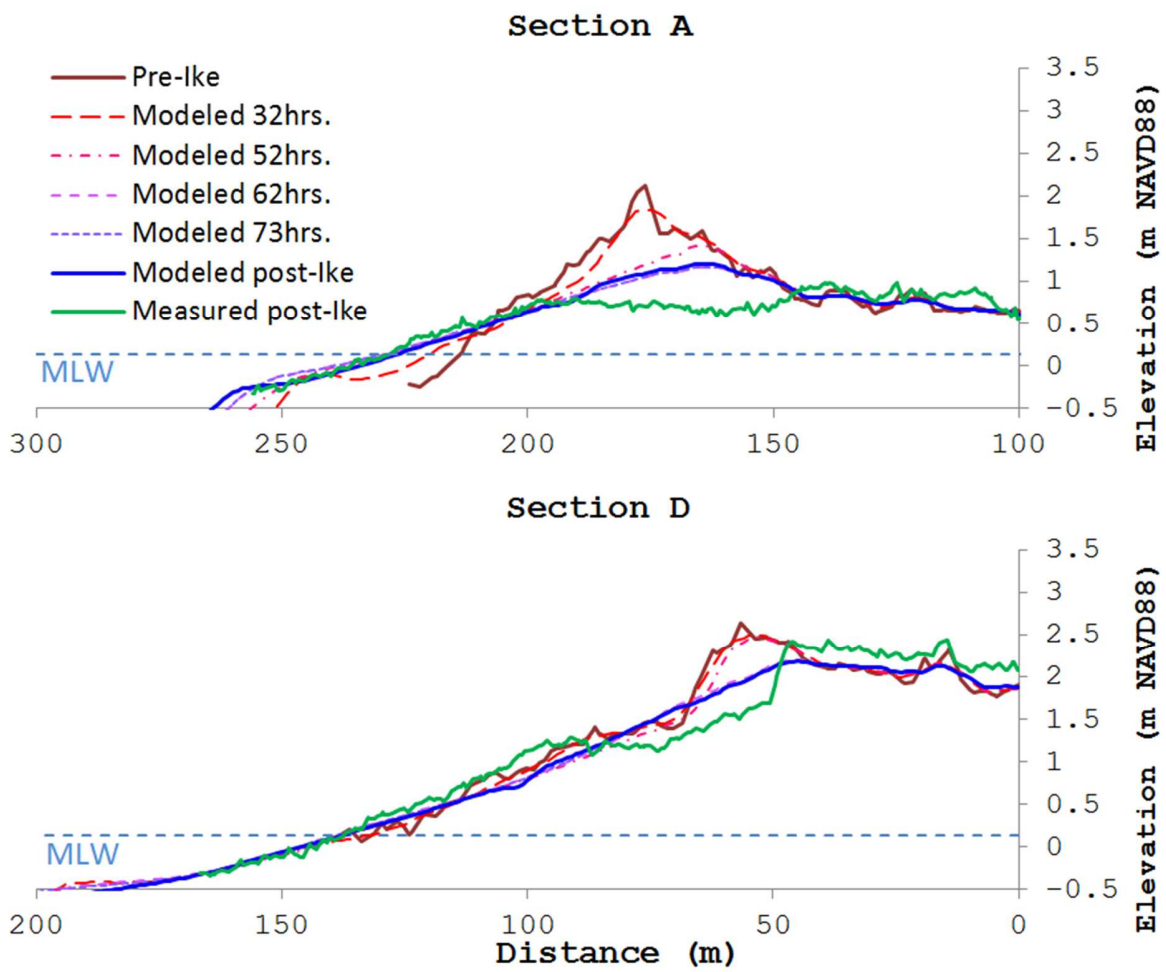


Fig. 11: CSHORE simulated bed level evolution compared to pre- and post-storm bed level extracted from LiDAR data at Sections A (the east end of FI) and Section D (near the center of FI).

Table 1: Xbeach smax sensitivity testing on Section A. Total eroded and accreted sediment volume in XBeach with varying smax values.

smax	Computation time [min.]	Total Volume Accreted [m ³ /m]	Total Volume Eroded [m ³ /m]
No Limit	4.9	3.10	-35.87
1.2	5.0	10.58	-17.02
1.0	4.8	10.44	-14.17
0.8	4.8	9.14	-11.26

Table 2: XBeach simulated volume of subaerial accretion and erosion at the end of the collision regime (32 hrs.), the overwash regime (52 hrs.), the inundation regime (62 hrs.), the storm surge ebb (73 hrs.), and at the end of the model (96 hrs.).

	Volume accreted [m ³]	Accretion rate [m ³ /hr]	Volume eroded [m ³]	Erosion rate [m ³ /hr]	Net volume change [m ³]
32 hrs.	+359,252	+11,226	-325,601	-10,175	+33,651
52 hrs.	+598,407	+11,957	-519,788	-9,709	+78,618
62 hrs.	+914,301	+31,589	-820,441	-30,065	+93,860
73 hrs.	+1,103,664	+17,214	-1,055,741	-21,390	+47,923
96 hrs.	+1,181,603	+3,388	-1,147,824	-4,003	+33,779
LiDAR	+1,430,593		-833,440		+597,153

Table 3: XBeach simulated volume of accretion and erosion at Section-D at the end of the collision regime (32 hrs.), the overwash regime (52 hrs.), the inundation regime (62 hrs.), the storm surge ebb (73 hrs.), and at the end of the model (96 hrs.).

	Volume accreted [m ³ /m]	Accretion rate [m ³ /m-hr]	Volume eroded [m ³ /m]	Erosion rate [m ³ /m-hr]	Net volume change [m ³ /m]
32 hrs.	+5.7	+0.18	-6.8	-0.21	-1.1
52 hrs.	+6.2	+0.03	-7.9	-0.06	-1.7
62 hrs.	+7.3	+0.11	-18.3	-1.04	-11
73 hrs.	+6.0	-0.12	-27.6	-0.85	-21.6
96 hrs.	+5.7	-0.01	-29.6	-0.09	-23.9

Table 4: CSHORE simulated volume of accretion and erosion at Section-D at the end of the collision regime (32 hrs.), the overwash regime (52 hrs.), the inundation regime (62 hrs.), the storm surge ebb (73 hrs.), and at the end of the model (96 hrs.).

	Volume accreted [m ³ /m]	Accretion rate [m ³ /m-hr]	Volume eroded [m ³ /m]	Erosion rate [m ³ /m-hr]	Net volume change [m ³ /m]
32 hrs.	+2.5	+0.08	-3.8	-0.11	-1.3
52 hrs.	+3.1	+0.02	-9.3	-0.17	-6.2
62 hrs.	+5.2	+0.10	-13.1	-0.19	-7.9
73 hrs.	+4.8	-0.04	-13.8	-0.07	-9.0
96 hrs.	+4.5	-0.01	-13.7	+0.01	-9.2

Table 5: Skill and bias of CSHORE and XBeach simulations for Sections A-H.

	CSHORE		XBeach	
	Skill	Bias [m]	Skill	Bias [m]
Section A	0.629	0.007	0.789	0.016
Section B	0.388	0.655	0.811	0.100
Section C	0.283	0.380	0.670	-0.069
Section D	0.496	-0.051	0.326	-0.041
Section E	0.413	-0.005	-0.109	-0.026
Section F	0.382	-0.038	-0.374	-0.049
Section G	0.087	-0.164	-0.040	-0.125
Section H	-0.109	-0.055	0.000	0.075
Total	0.345	0.170	0.491	0.002